J. Fluid Mech. (1981), *vol.* 110, *pp.* 433–456
Printed in Great Britain

Convection in rectangular cavities with differentially heated end walls

By P. G. SIMPKINS AND T. D. DUDDERAR
Bell Laboratories, Murray Hill, New Jersey 07974

(Received 29 September 1980)

This paper describes an experimental study of free convection in an enclosed rectangular cavity, the end walls of which are maintained at uniform but different temperatures. The experiments are carried out for a variety of Rayleigh numbers, $R = \alpha g \Delta T h^4/\kappa \nu l$, and aspect ratios, $L = l/h$, for fluids with Prandtl number $\sigma \geqslant 10$. For $R \sim O(10^3)$ it is shown that the basic structure of the flow field is a single two-dimensional cell for $0{\cdot}25 \leqslant L \leqslant 9$. When $R > O(10^4)$ the boundary layers on the vertical walls control the flow field, but the basic overall structure remains unicellular. At greater values of R secondary vortices appear for all $L \geqslant 0{\cdot}5$. As R increases the intensity and then the number of these vortices increases. Measurements of the end-wall boundary-layer profiles at different values of R and L confirm Gill's boundary-layer analysis. The effects of variations of viscosity with temperature are discussed in the context of the observed boundary-layer profiles.

Core shear profiles and mass flux measurements are also reported. For $L = 1$ the observed shear profiles are in good agreement with numerical solutions of the Boussinesq equations. However, when $L > 1$ the observations suggest that the horizontal boundary layers have a significant effect on the core flow field. The stream function is demonstrated to be L-dependent in the boundary-layer regime, where variations due to R are second order. Similarities between the results of the present work and earlier observations by Elder and by Seki, Fukusaka & Inaba for tall slender cavities ($L \ll 1$) are discussed.

1. Introduction

When a fluid is subjected to a horizontal temperature gradient, motion is generated even for temperature differentials which are infinitesimally small. The explanation for this motion follows from hydrostatics, see Landau & Lifshitz (1959). If the temperature distribution in a fluid in a gravitational field is a function of any co-ordinate other than the vertical, there is no pressure distribution to balance the thermally induced buoyancy force. The simplest steady state is the single two-dimensional cell that occurs when the applied temperature gradient is a function of one horizontal component. Then the fluid rises in the region of greatest heating, and moves towards the cooler region where it descends and returns to its original position. When the aspect ratio L is large, end effects can be neglected; this simple shearing motion is known to meteorologists as a Hadley cell in recognition of Hadley's (1735) pioneering paper on atmospheric circulations.

Compared with the understanding developed on the Rayleigh–Bénard system, the present understanding of the motion induced by a temperature gradient normal to gravity is much more rudimentary. Some features of the flow field were derived by Batchelor (1954) who obtained estimates of the Nusselt number for the conduction regime, $R \to 0$, and the intermediate regime, $R \leqslant O(10^4)$. He also demonstrated that the flow is uniquely determined by three parameters: the Rayleigh number R, the Prandtl number σ, and the aspect ratio L. At large Rayleigh numbers, $R \sim O(10^5)$, Batchelor asserted that the flow consists of a core of constant temperature and vorticity surrounded by thermal and viscous boundary layers on the cavity walls. However, the experimental observations of Eckert & Carlson (1961) and Elder (1965) demonstrated conclusively that, in tall slender cavities ($L < 1$), the core is vertically stratified. Later Singh & Cowling (1963) and Gill (1966) in analytical studies, and de Vahl Davis (1968) in a numerical study showed that for $R \geqslant O(10^5)$ the boundary layers on the vertical walls were compatible with a core which is vertically stratified. The stability of a Hadley cell was originally discussed by Hart (1972) who showed that for rigid conducting boundaries the transverse modes were always the most unstable. Two types of instability were found to occur, a convective instability when $\sigma > 0{\cdot}05$ and a shear instability when $\sigma < 0{\cdot}05$. More recently, Gill (1974) extended Hart's analysis to the limit $\sigma \to 0$, and predicted that oscillatory behaviour would occur beyond a critical Rayleigh number $R_c > 1030$. Also in 1974 Cormack, Leal & Imberger developed an end-wall correction for the Hadley cell. These authors found that for large but finite aspect ratio cavities the core stream function is proportional to that of the Hadley solution. The proportionality constant K is given by

$$K = 1 - 3{\cdot}48 \times 10^{-6} R^2 L^{-1}. \tag{1.1}$$

Since the correction term must be small compared to unity the Hadley-cell description is valid when $L \gg 3{\cdot}48 \times 10^{-6} R^2$.

A number of experimental studies have demonstrated that thermal oscillations occur in low-Prandtl-number fluids when a critical value of the Rayleigh number is exceeded. Observations have been reported for sodium chloride (Utech & Flemings 1966), mercury (Pamplin & Bolt 1976), tin (Cole & Winegard 1964), gallium (Hurle, Jakeman & Johnson 1974) and indium antimonide (Müller & Wilhelm 1964). Hurle (1966) has reported on the relationship of such thermal oscillations to undesirable growth striae that occur in the manufacture of some semi-conductor materials. Some of these observers have also noted the strong dependence of the periodicity of the oscillations on the aspect ratio. Hurle *et al.* (1974) in particular have found that the periodicity is proportional to the aspect ratio. In these latter experiments $L \simeq 3$ and the critical Rayleigh number was observed to be approximately $3{\cdot}5 \times 10^3$. The Hadley approximation is inappropriate for these conditions, since it follows from equation (1.1) that $L \gg 40$. In fact in most crystal-growth applications L is too small for the Hadley approximation to be valid. Consequently, the Gill (1974) stability analysis, which represents the limiting behaviour as $L \to \infty$, is also inappropriate.

The results presented here demonstrate that the natural convection in a confined cavity due to a horizontal temperature gradient is significantly different when the aspect ratio $L \gg 1$ from that when $L \ll 1$, once a critical Rayleigh number R_c is exceeded. Here, the aspect ratio $L = l/h$, where l is the length and h is the height of the cavity. The difference between these two states is easily seen by comparing the photo-

graphs taken by Elder (1965) with those presented here at supercritical Rayleigh numbers. Beyond R_c the steady unicellular flow breaks down into a series of vertically aligned rolls when $L \ll 1$, whereas when $L > 1$ rolls are observed only close to the end walls; these intensify with increasing R but do not extend further into the core.

2. Theoretical background

The principal work on the steady convection in an enclosed cavity due to a horizontal temperature gradient is by Gill (1966). When the Rayleigh number is large, boundary layers exist on the vertical end walls of the cavity. Gill (1966) showed that after appropriate scalings are introduced neither the boundary-layer nor the core solution are, to first order, dependent on R or L. In the high-Rayleigh-number limit the core temperature is vertically stratified, i.e. $T = T_\infty(z)$, rather than isothermal as Batchelor (1954) had assumed. Further Gill showed that the vertical boundary layers are $O[R^{-\frac{1}{4}}L^{-\frac{5}{4}}l]$ in thickness and have a characteristic velocity $O[R^{\frac{1}{2}}L^{\frac{3}{2}}\kappa/l]$. For the analysis to be valid, the boundary-layer thickness must be small compared with the cavity length. In the present notation this criterion is satisfied when

$$11{\cdot}5R^{-\frac{1}{4}}L^{-\frac{5}{4}} < 1. \tag{2.1}$$

A crucial assumption in the solution given by Gill (1966) is that the effect of the flow near the horizontal surfaces is negligible. Physically, this assumption implies that most of the fluid in the vertical boundary layers empties into the core. For cavities of aspect ratio $L < 1$ the assumption is plausible, since the flow is predominantly vertical. However, when $L > 1$ the flow is essentially horizontal, except near the end walls. An active role is still played by the vertical boundary layers but intuitively it would seem that for constant R the role of the horizontal layers would increase proportionately with the aspect ratio L.

The residence time of a particle in the core is a measure of the circulation time, since the residence time in the vertical boundary layers is small. A particle will traverse a cavity in a time

$$t' = \int_0^l \frac{dx'}{u'} = O[h^2L^{\frac{3}{4}}/\kappa R^{\frac{1}{4}}].$$

For gallium arsenide, a semi-conductor substrate material, the thermal diffusivity $\kappa \sim 0{\cdot}04$ cm^2 s^{-1} so that in a typical industrial crucible ($l \sim 20$ cm, $h \sim 2{\cdot}5$ cm and $R \sim 10^4$) the circulation time $t' \sim O(10^2\text{s})$. This is negligible compared with the growing time of a crystal ~ 20 hours, and thus the flow in the melt can be considered to be steady.

Another property of the equations and boundary conditions is that they are unaltered by a simultaneous change of sign of the three variables, $T' - (\frac{1}{2}T'_w)$, $x' - (\frac{1}{2}l)$ and z', while the sign of the fourth variable ψ is unchanged. This is the property involving a reflection about the cavity centre $x' = \frac{1}{2}l$, $z' = \frac{1}{2}h$ which Gill (1966) termed centro-symmetry. Thus the core temperature, T_∞, is an odd function and the core stream function, ψ_∞, an even function about $z' = \frac{1}{2}h$. In the notation adopted by Blythe & Simpkins (1977) the centro-symmetry conditions are

$$\psi(x, z) = \psi(L-x, 1-z), \tag{2.2}$$

$$T(x, z) = L - T(L-x, 1-z), \tag{2.3}$$

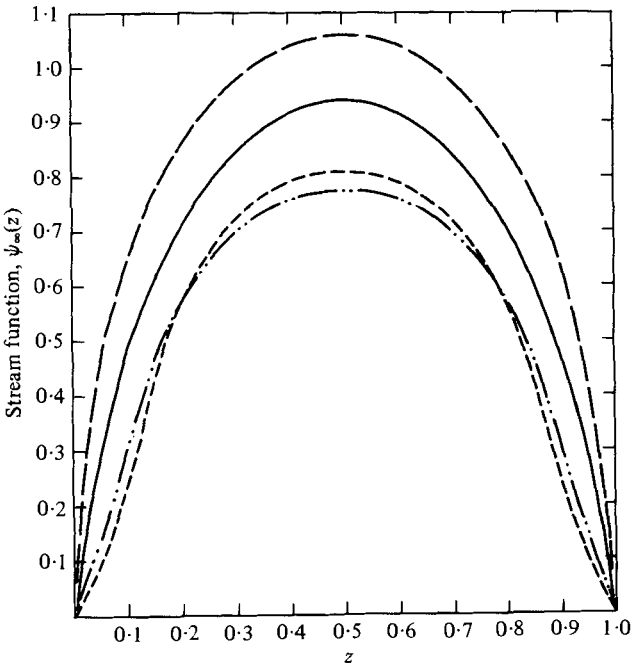

FIGURE 1. Analytical predictions of the core stream functions based on the boundary-layer equations compared with numerical solutions of the Boussinesq equations. $R \sim 10^6$, $L = 1$. — —, Gill, $\sigma = \infty$; ——, integral method, $\sigma = \infty$; - - -, Quon, $\sigma = 7{\cdot}1$; —·—, Stewart & Weinberg, $\sigma = 10$.

where x and z are the non-dimensional horizontal and vertical co-ordinates, respectively.

The approximate forms of the Navier–Stokes equations valid in the vertical boundary-layer regions are, in the usual non-dimensional variables,

$$u = \psi_z, \quad w = -\psi_x, \tag{2.4a}$$

$$(1/\sigma)(uw_x + ww_z) = w_{xx} + T - T_\infty(z), \tag{2.4b}$$

$$uT_x + wT_z = T_{xx}, \tag{2.4c}$$

where $T(\infty, z) = T_\infty(z)$ and the Boussinesq approximation has been made. It was shown in Blythe & Simpkins that for $\sigma \to \infty$ equations (2.4) have similarity solutions

$$\psi = \psi_\infty(z) H(\eta), \quad T = T_\infty(z) G(\eta), \tag{2.5}$$

where $\eta = x/\delta(z)$ and δ is a suitable boundary-layer thickness. A brief discussion of these solutions is given in appendix A.

Both Singh & Cowling (1963), in a paper which seems to have been previously overlooked, and Gill (1966), used rather simple methods to integrate the boundary-layer equations. Consequently, when their results are compared with numerical solutions of the Boussinesq equations, e.g. see Quon (1972; see also Cormack & Leal 1974) and Stewart & Weinberg (1972), discrepancies arise which cannot be explained unambiguously. Recently, Blythe & Simpkins (1977) developed an integral method for solving the boundary-layer equations which improved on the earlier results. Good

agreement between the numerical predictions and the integral method was found for the temperature distribution but a discrepancy in the core stream-function distribution remained unresolved. Figure 1 shows the differences between the analytical solutions of the boundary-layer equations and the numerical solutions of the Boussinesq equations for $R \sim O(10^6)$ and $L = 1$. The non-dimensional core stream function, ψ_∞, is defined as

$$\psi_\infty = \psi'[\kappa R^{\frac{1}{4}} L^{\frac{1}{4}} b^{\frac{3}{4}}]^{-1},$$

where b is a constant determined from the boundary-layer profile. Throughout this paper the constant, $b = 0{\cdot}630$, corresponds to the similarity solution

$$F(\eta) = 2e^{-\eta} \sin \eta, \tag{2.6}$$

see appendix A. The discrepancy between the integral method and the numerical results has been attributed to the boundary-layer approximation of the Boussinesq equations. Simpkins & Blythe (1980) demonstrated this by applying the integral technique to the equivalent problem for a fluid-saturated porous medium for which numerical solutions to the boundary-layer equations had been given by Walker & Homsy (1978). In this case the core stream-function distribution predicted by the integral method for three boundary-layer profiles was in excellent agreement with the numerical solutions.

Another simplification in the Gill (1966) analysis, the assumption that the horizontal boundary layers may be neglected, has been questioned by Quon (1972; see also Cormack & Leal 1974). Although the boundary conditions $\psi = 0$ at $z = 0, 1$ are exact for the Boussinesq equations, it is not clear *ab initio* that the core will satisfy these conditions. Solutions based on the boundary-layer assumption have singularities at $z = 0, 1$ leading to infinite vertical temperature gradients and infinite horizontal velocity components at these boundaries. Quon (1972) used various boundary conditions on the horizontal surfaces to examine their effect on the vertical boundary-layer and core solutions, and found that such changes produced only second-order effects. Thus, Quon was unable to attribute the large discrepancy he found in the core stream function compared with Gill, see figure 1, to variations in the horizontal boundary conditions. Quon (1972, 1977) and Roux *et al.* (1978) have discussed various ways of choosing a value for the free constant C used in the Gill analysis to improve the solution. None of these approaches were completely successful.

Matching between the flow in the vertical boundary layers and the core, far from the corners, is now understood for large-Prandtl-number fluids. In this case the boundary layers on the horizontal walls do not play an important role. However, no scaling of the governing equations for the structure near the horizontal walls has been given that is consistent with the core behaviour. This difficulty is amplified when small- or moderate-Prandtl-number fluids are considered because the core structure is then strongly dependent on the horizontal matching conditions. Such flows are predominantly associated with molten metals and semi-conductor materials. Before an appropriate stability analysis can be undertaken, therefore, more realistic representations of the steady-state flow fields in the various Prandtl-number regimes must be developed.

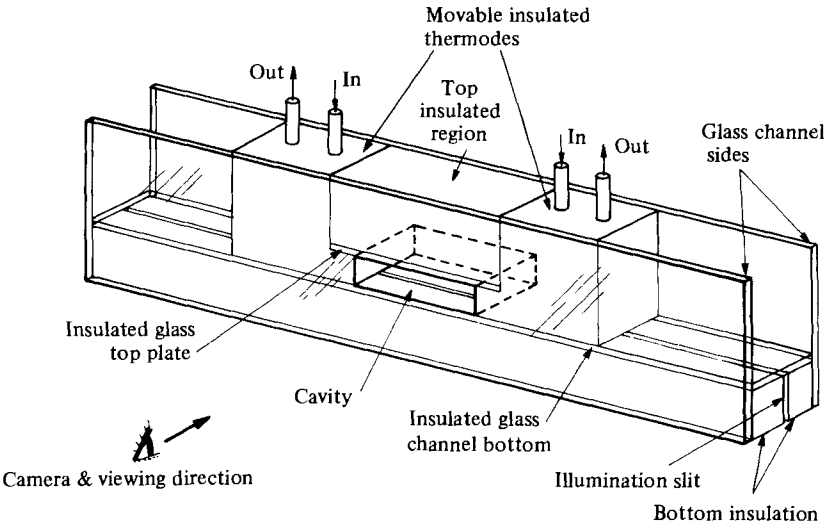

FIGURE 2. Schematic representation of the experimental apparatus.

3. Experimental methods

The convective motions under investigation were established in an enclosed rectangular cavity (see figure 2) the vertical end walls of which could be laterally adjusted to alter the cavity length. The height, h, and breadth, b, of the cavity were fixed at 20 mm and 50 mm, respectively. The end walls were made from solid copper blocks with individual copper chambers behind them that were encased in insulating foam. These assemblies are referred to as thermodes. Water at constant temperature was pumped from two thermostatically controlled baths through the end-wall thermodes, thus allowing a temperature difference ΔT to be maintained across the cavity to within an accuracy of $\pm$ 0·25 °C. The top and bottom surfaces of the cavity were 2 mm glass plates covered with at least 3 cm of polystyrene insulation. A slit in the bottom insulator midway across the breadth of the cavity allowed a collimated sheet of light into the interior for illumination. The side walls were 2 mm thick glass plate that were externally insulated; a small removable section on one of the lateral insulating walls allowed access for visual observations.

In these studies the test fluids used were silicone oils with viscosities of 10, 100, 500 and 1000 cSt (10^{-2} cm^2 s^{-1}); their physical properties are tabulated in appendix B. Such viscous oils also have large Prandtl numbers. To be consistent with the 'simplified' Boussinesq approximation the physical properties of the fluids should be independent of the temperature and $\alpha\Delta T \ll 1$ (Joseph 1976). With the exception of the variation of viscosity with temperature, which is significant, these requirements are satisfied. Unless otherwise stated the Rayleigh numbers quoted in the results are computed with the viscosity data evaluated for convenience at 25 °C, as given by the manufacturer. At some of the larger values of ΔT the local viscosity near the hot wall is significantly reduced and noticeable asymmetries develop in the flow. At the largest Rayleigh numbers examined, the temperature difference ΔT across the end walls is about 80 °C. At the cold wall temperature, the viscosity is then four times greater than the viscosity at the hot wall temperature. However, since the important parameter

in the vertical boundary-layers solutions is $R^{\frac{1}{4}}$, the significance of the variations in ν is reduced to a maximum of $\pm 20\,\%$ about a mean value.

The finite breadth of the cavity leads to another departure from the idealized two-dimensional flow field. Elder (1965) has noted, however, that for sufficiently large R the motion is closely two-dimensional even when $l/b = 1$. The relevant parameter is δ^*/b, where δ^* is a boundary-layer thickness. Provided this ratio is small, three-dimensional effects are negligible away from the side walls. In the work reported all data were taken midway across the cavity. The thickness of the illuminated plane was restricted to about 2 mm, which was substantially greater than the depth of field of the recording instruments.

Flow-visualization studies were performed with cavities of aspect ratio $0{\cdot}25 \leqslant L \leqslant 9$ for a variety of Rayleigh numbers. Various tracer elements were used to provide the side scattering of the illuminating sheet of light. These included aluminium powder, styrene particles, and latex paint. The choice of tracer material depended on the viscosity of the fluid in the cavity. An $f2.8$, 50 mm lens, set for a magnification of about two, was used to record the flow fields. Exposure times for the photographs, taken with 3000 ASA Polaroid film, were typically between 15 and 30 s. Steady-state conditions were examined for periods up to 24 h. In general it was found that the flow in the silicone oils responded to a temperature change in approximately 0·5 h.

Local measurements of the velocity components were obtained by recording the transit time of a particle over a known distance. Particles were observed with a travelling microscope, through which motions over a distance as small as 0·12 mm could be observed. Time intervals were taken with a digital clock accurate to 0·01 s and the (x, z) location of the microscope was controlled by micrometers with vernier scales. Generally, the shear profile data were recorded only at the mid-plane of the cavity. However, for one particular aspect ratio, $L = 4$, observations were made at other lateral positions equidistant from the mid-plane.

Measurements of the velocity distribution across the depth of the cell have been made for aspect ratios of 1, 2, 4 and 8·9. These data were recorded for various Rayleigh numbers, and an effort was made to obtain the same value of R with different aspect ratios. Sometimes this was accomplished by changing the fluid in the cell to broaden the viscosity range. Thus variations in the Prandtl number, σ, were introduced in some tests. The effect of this variation in σ on the velocity distributions is expected to be small because all of the liquids used have Prandtl numbers greater than ten. Quon (1972) has shown that $\sigma > 10$ is equivalent to the limiting value $\sigma \to \infty$.

Observations of the velocity distribution in the vertical boundary layers were made at the cavity mid-height. At each position a minimum of five separate observations were made, and the velocity was calculated from their mean. The accuracy of these data is believed to be within $\pm 2\,\%$.

One additional comment is in order. All the experiments reported satisfy the Gill (1966) criterion that the vertical boundary layers are small compared with the cavity length, i.e. $RL^5 > 2 \times 10^4$. Thus, the results to be discussed below are ostensibly for the boundary-layer regime in large-Prandtl-number fluids. Consequently, the number of parameters to be varied is reduced from three to two, i.e. R and L.

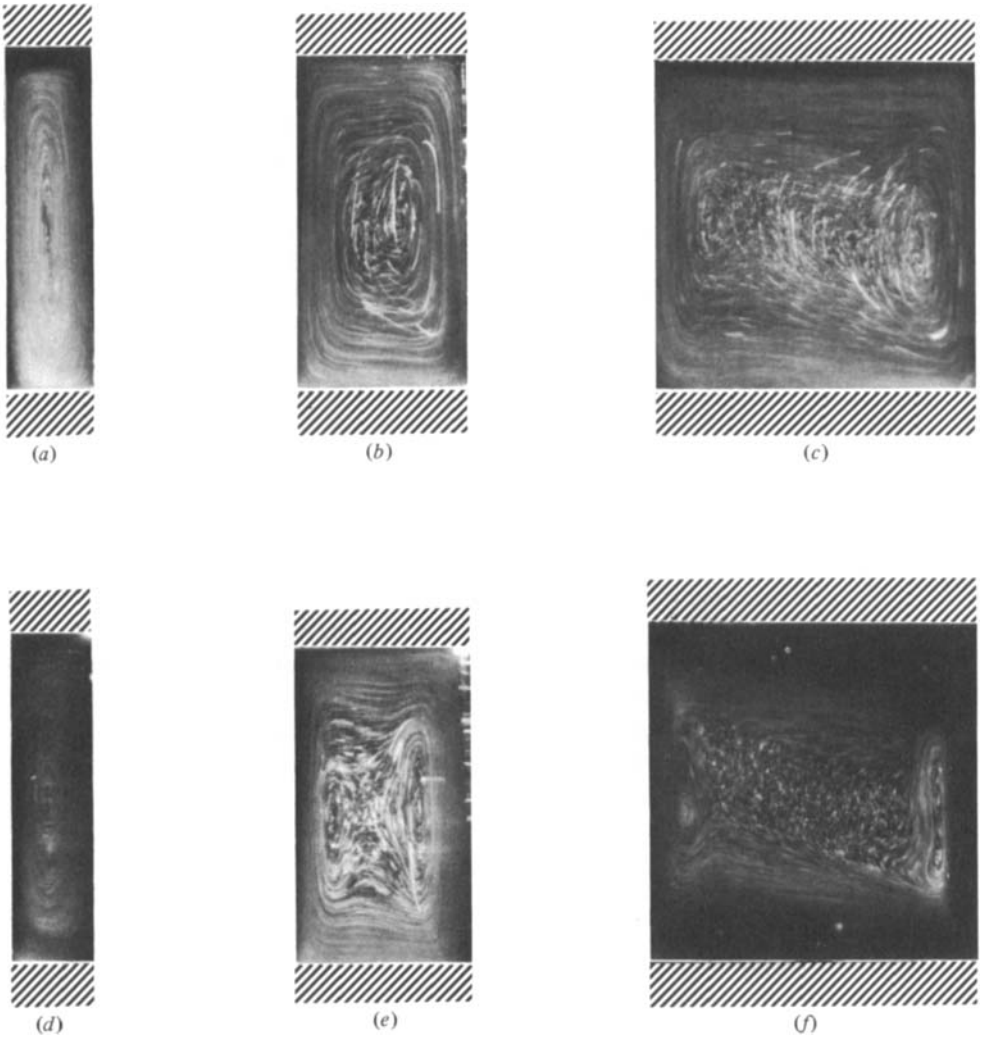

FIGURE 3. Streak photographs of the flow fields in the cavities of aspect ratio $L = \frac{1}{4}$, $\frac{1}{2}$ and 1. The Rayleigh numbers in millions are (*a*) 2·71, (*b*) 1·35, (*c*) 0·68, (*d*) 10·8, (*e*) 2·71 and (*f*) 2·71. The viscosity $\nu = 10$ cSt and the cell height $h = 2$ cm.

4. Results and discussion

4.1. *Flow visualization*

Figures 3–5† show the combined effects of changing the Rayleigh number and the aspect ratio on the flow field in the cavity. These, and other pictures, show that when $R < R_c$ the primary flow field is a single cell.

Another feature common to all the photographs is the entrainment and detrainment of the flow in the vertical boundary layers. Notice that on the lower half of the cold wall mass is ejected from the vertical boundary layer into the region adjacent to the horizontal surface. The horizontal layer converges toward the lower corner of the hot

† In all the photographs the cold wall is on the left and the hot wall on the right of the pictures.

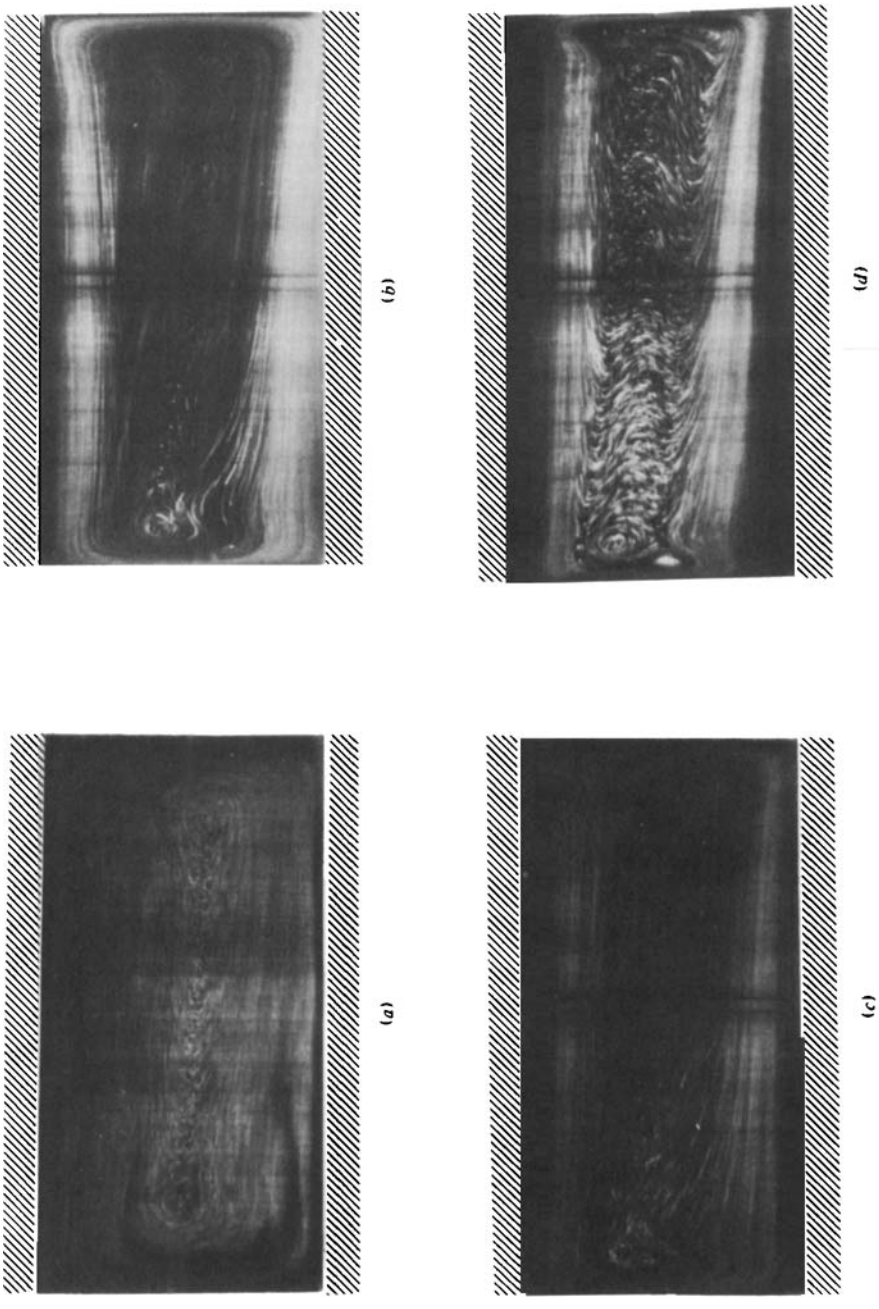

FIGURE 4. Streak photographs of the flow fields in a cavity of $L = 2$. The Rayleigh numbers in millions are (*a*) 0·06, (*b*) 0·66, (*c*) 1·17 and (*d*) 2·90. The viscosity $\nu = 10$ cSt, and the cell height $h = 2$ cm.

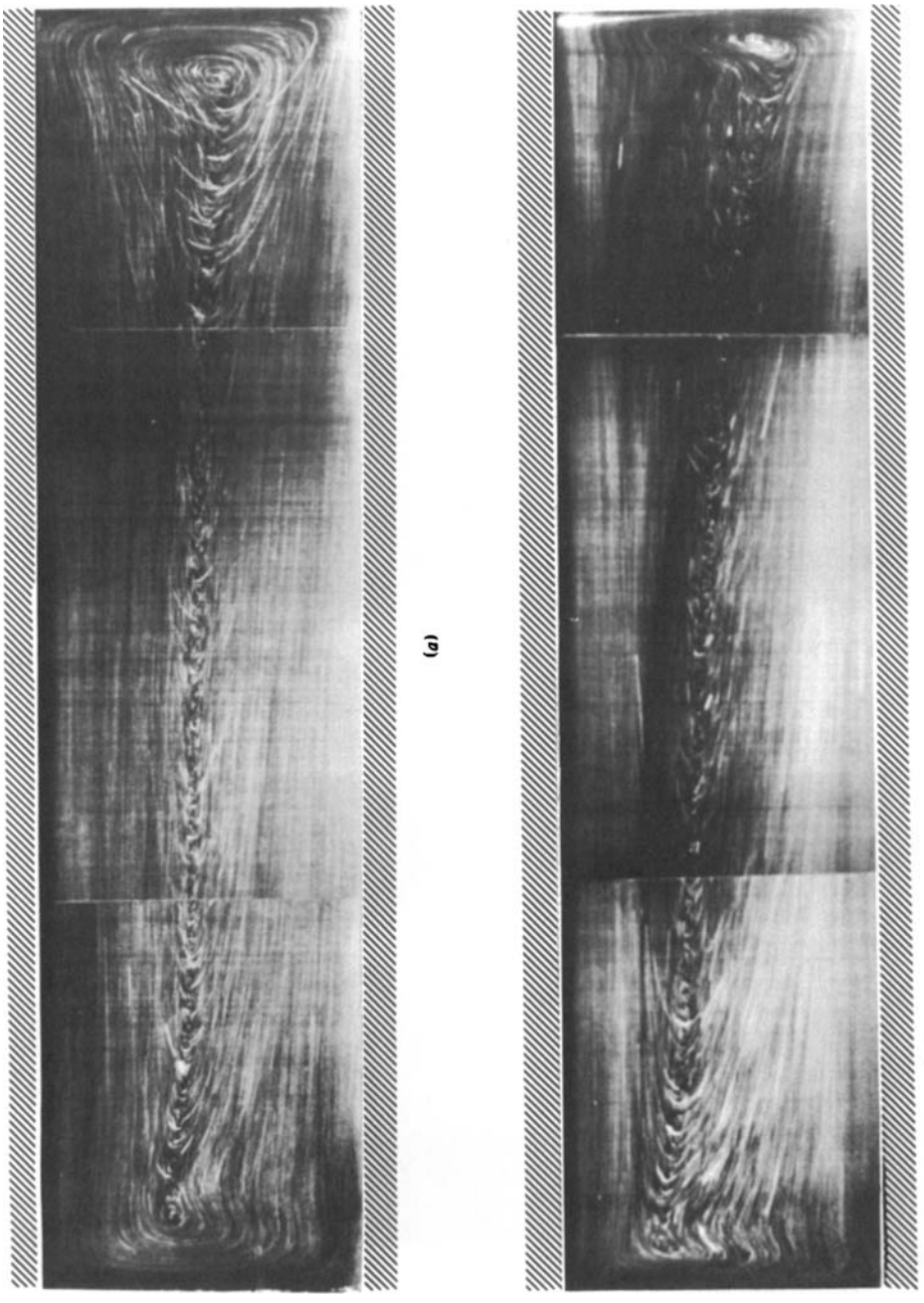

FIGURE 5. Streak photographs of the flow field in a cavity of $L = 4$. The Rayleigh numbers in millions are (*a*) 0·23 and (*b*) 0·91. The viscosity $\nu = 10$ cSt and the cell height $h = 2$ cm.

wall and is then swept upward into the vertical boundary layer. Similar features are to be seen at the upper half of the hot wall, illustrating the centro-symmetry pointed out by Gill. In figure 3 the flow in the narrowest cavity ($L = 0{\cdot}25$) remains a single cell up to $R = 1{\cdot}08 \times 10^7$. This observation is consistent with Elder's data where secondary flows were found to occur for $RL^4 \simeq 3 \times 10^5 \pm 30\,\%$ in a cavity with $L = 0{\cdot}0526$. When $L = 0{\cdot}5$ a weak secondary flow appears at $R = 1{\cdot}35 \times 10^6$ and intensifies into a distinct vortex structure by $R = 2{\cdot}71 \times 10^6$. Note that two elongated vortices occur parallel to the vertical walls and are embedded in the primary circulation. When L is increased to unity the secondary flow becomes evident at $R = 6{\cdot}8 \times 10^5$. The motion in these vortices intensifies with increasing R until at $R = 2{\cdot}71 \times 10^6$ a subsidiary pair of vortices develops within each roll of the secondary flow. In figure 3 the effect of aspect ratio variations on the flow at fixed $R\,(= 2{\cdot}71 \times 10^6)$ are clearly seen. Within the boundary-layer regime, where $(RL^5)^{0{\cdot}25} > 11{\cdot}5$, the layers adjacent to the vertical walls are obviously much thinner than those along the horizontal surfaces. The very slow motion that occurs in the core is evident from the individual particles which are almost stationary. In the corner regions the scale on which the flow is entrained into the horizontal layers from the ejecting vertical boundary layers is about one quarter of the cavity height. These corner flows are significantly affected by the secondary motion, when it occurs, because the fluid is ejected almost from the mid-height region of the core. In other words the vortex near the vertical wall causes the flow to turn away from the corner before it enters the horizontal boundary layer.

Figure 4 shows the Rayleigh number dependence for a cavity with an aspect ratio of 2. The basic unicellular circulation for $R \sim O(10^4)$ develops a secondary flow about $R = 6{\cdot}6 \times 10^5$. Once again the secondary flow intensifies with increasing R until at about $R = 1{\cdot}8 \times 10^6$ subsidiary vortices appear parallel to each vertical wall. At $R = 2{\cdot}9 \times 10^6$ three vortices are evident near each vertical wall and there is significant two-dimensional flow in the core. The lack of centro-symmetry in the flow is attributed to the variation of viscosity with temperature.

Examples of the flows at an aspect ratio $L = 4$ are given in figure 5. The range of R covers the region from predominantly unicellular motion at $R = 2{\cdot}3 \times 10^5$ into the secondary flow state which is well established at $R = 4{\cdot}5 \times 10^5$. The flow field for $R = 9{\cdot}1 \times 10^5$, $L = 4$ resembles that observed at $R = 1{\cdot}17 \times 10^6$, $L = 2$; throughout most of the core region it appears to be a vertically stratified shear flow.

4.2. *The vertical boundary-layer profiles*

Figure 6 shows two of the boundary-layer profiles recorded near the hot wall for different values of R and L. Within the experimental uncertainty the data are coincident. These results confirm Gill's prediction that the solutions are independent of the Rayleigh number and aspect ratio. Also shown in the figure is the function $F(\eta)$ used by Blythe & Simpkins (1977) and the numerical prediction due to Quon (1972). The agreement between the integral method of Blythe & Simpkins and Quon's numerical solution to the Boussinesq equations is good, but both predictions are significantly less than the observations when $\eta \leqslant 1{\cdot}0$. This difference is attributable to the temperature-dependent viscosity which the silicone oils exhibit. If the data for $\nu = 1000$ cSt are evaluated with a reduced viscosity of 570 cSt based on the hot wall temperature, the amplitude of the velocity profile is significantly altered, see figure 7. Near the wall, $\eta < 0{\cdot}5$, the modified data are in good agreement with the theoretical curve, but

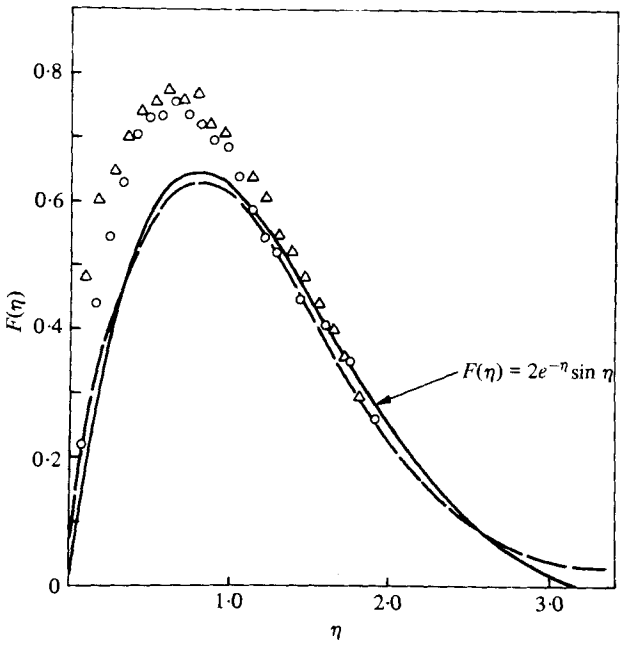

FIGURE 6. Boundary-layer observations at different Rayleigh numbers and aspect ratios compared with analytical and numerical predictions. ○, $R = 2{\cdot}18 \times 10^4$, $L = 1$; △, $R = 0{\cdot}75 \times 10^4$, $L = 4$; — —, Quon, $\nu = 1000$ cSt.

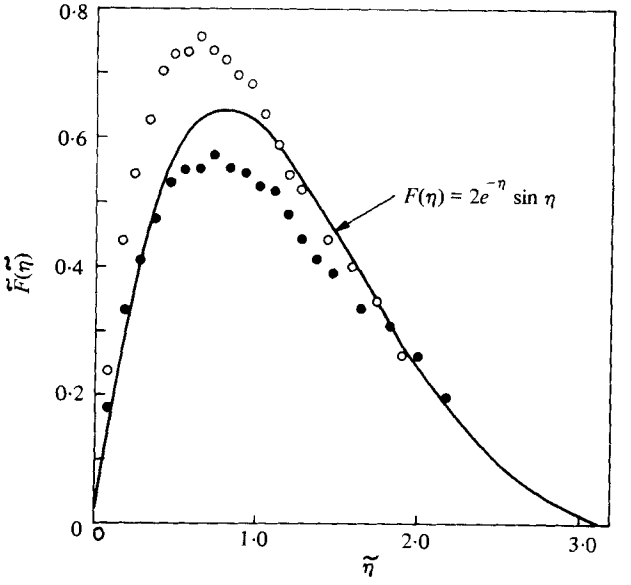

FIGURE 7. The effect of using a reduced viscosity ν (at the hot-wall temperature) on the vertical boundary-layer observations. ○, $R = 2{\cdot}18 \times 10^4$, $\nu = 1000$ cSt; ●, $R = 3{\cdot}83 \times 10^4$, $\nu = 570$ cSt; $\eta = 1{\cdot}151\eta$, $L = 1$.

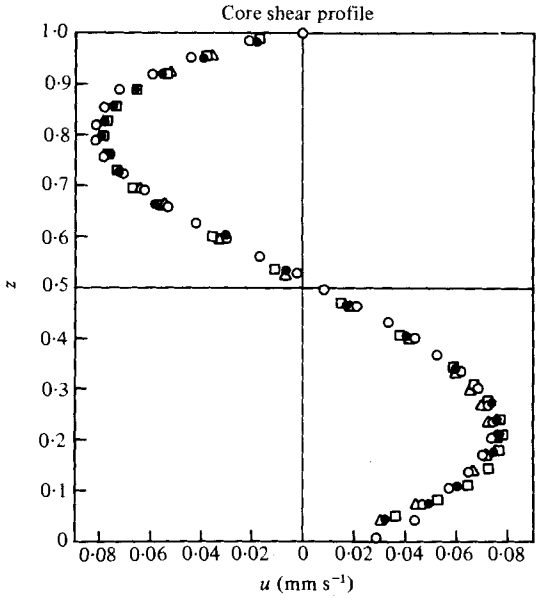

FIGURE 8. Core shear profile at various longitudinal locations, $R = 3{\cdot}34 \times 10^3$, $L = 4$, $\Delta T = 17{\cdot}7$ °C, $\nu = 1000$ cSt, $\sigma = 10^4$. x' (mm): ○, 15·0; ●, 39·3; □, 59·6; △, 200.

when $\eta > 0{\cdot}5$ the discrepancy develops. As the core is approached, $\eta > 1{\cdot}0$, the data evaluated with $\nu = 1000$ cSt are in better agreement with the theoretical curve. Thus, near the wall the viscosity is reduced because of the high temperature but, as the temperature decreases further from the wall, a higher viscosity is appropriate. The fact that the two sets of values encompass the maximum of $F(\eta)$ suggests that variable viscosity effects can be significant and should be accounted for in future analyses.

4.3. *Core shear profiles*

Measurements of the velocity profiles at various longitudinal positions in a cavity of length $l = 80$ mm ($L = 4$) are shown in figure 8 for a moderate value of R. Two conclusions can be drawn from these data. First, the core shear profile is, to first order, independent of x. A very weak x-dependent trend is discernible in the data, but Gill's hypothesis that the core, to first order, is independent of R is clearly substantiated. Secondly, the layers near the horizontal surfaces are not vanishingly small; indeed, these horizontal layers fill the cavity from top to bottom. Although the Gill criterion for the vertical boundary layers is satisfied this is attributable to the large value of L, not to the value of R. The relatively low value of the Rayleigh number suggests that the flow field may be closer to the Batchelor conduction regime than the Gill boundary-layer regime. These comments will be amplified below.

When the Rayleigh number is increased to $R = 1{\cdot}35 \times 10^6$ the core shear profiles have a different character, see figure 9. These data illustrate the effect of varying L on the centre-line shear profile at fixed R. It is apparent that in this Rayleigh-number regime the layers near the horizontal surfaces are separated by a core region in which the velocity is very small. The vertical extent of core is inversely proportional to a function of the aspect ratio, being greatest for $L = 1$ and progressively decreasing until at $L = 4$ the horizontal layers are almost merged. Conversely, therefore, the horizontal

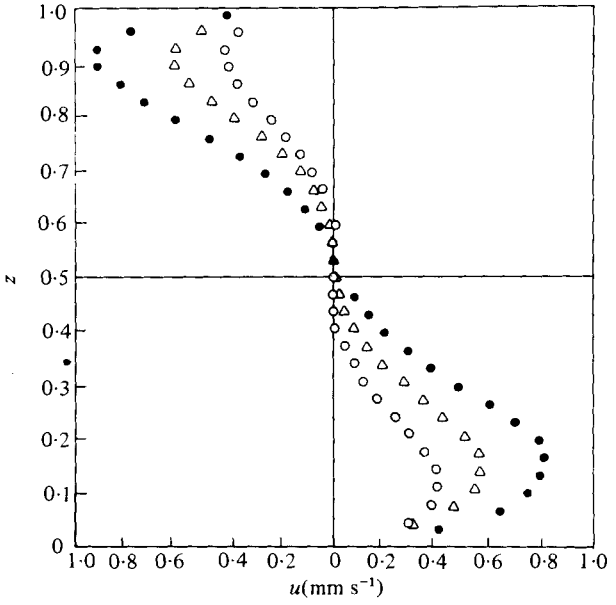

FIGURE 9. Core shear profiles for different aspect ratios, $R = (1{\cdot}35 \pm 0{\cdot}1) \times 10^6$, $\nu = 10$ cSt. ●, $L = 4$; △, $L = 2$; ○, $L = 1$.

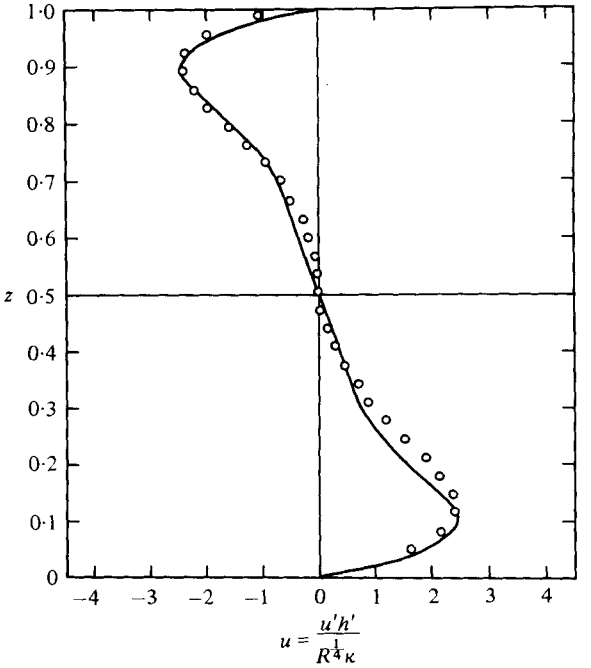

FIGURE 10. Comparison of the observed core shear profile with that predicted numerically, $L = 1$. ——, Quon, $R = 8 \times 10^5$, $\sigma = 7{\cdot}1$; ○, present data, $R = 7{\cdot}7 \pm 0{\cdot}3 \times 10^5$, $\sigma = 105$.

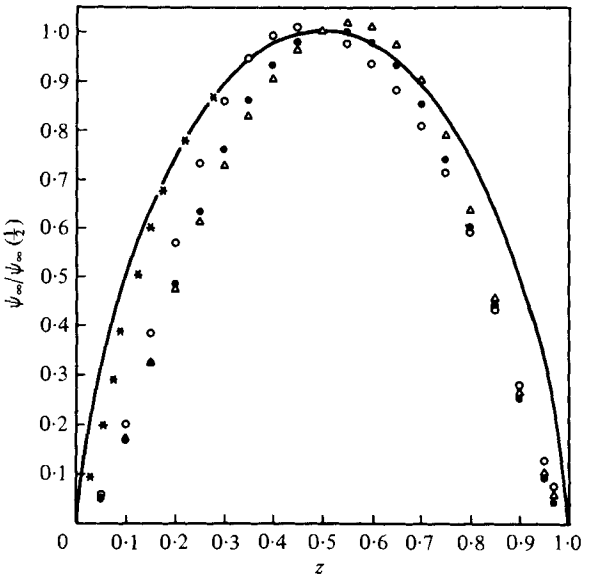

FIGURE 11. The normalized stream-function distributions compared with observations. $R = 7{\cdot}47 \times 10^5$, $L = 4$, $\nu = 10$ cSt, $\Delta T = 35{\cdot}4$ °C. x' (mm): ○, 59·6; ●, 39·3; △, 19·9. ——, integral method (boundary-layer equations); *, Stewart & Weinberg (numerical).

boundary layers are still a substantial portion of the cavity depth, and they grow with x, as might be expected. A comparison with the numerical predictions by Quon (1972) substantiates the present results and enhances confidence in the observations, see figure 10. The abscissa is the non-dimensional horizontal velocity component scaled with respect to $R^{\frac{1}{4}}$.

4.4. *Stream-function distributions*

The stream function profiles were obtained by using a least-squares routine to fit a polynomial of seventh degree or higher to the velocity measurements. The curve fit was integrated numerically and the local stream functions were evaluated at the depths corresponding to the measurements. Figure 11 shows a plot of the stream function normalized with respect to its value at $z = \frac{1}{2}$ compared with the numerical and integral methods. The overestimate of the analytical and numerical results is a manifestation of the differences in the magnitude of $\psi(\frac{1}{2})$. Plots of this type tend to be misleading because the disparities in the absolute values of the stream function are not apparent, cf. figure 1. The data do, however, illustrate the effect of centro-symmetry at this larger Rayleigh number. The skewness associated with the x-location arises because near the cold wall ($x = 0$) the horizontal layer near the bottom of the cell ($z = 0$) is thicker and the flow, therefore, slower than at the top of the cell ($z = 1$). Near the hot wall the reverse situation occurs. Similar characteristics are apparent from the velocity measurements, see figure 12.

Figure 13 shows the core stream function ψ_∞ variation with R at fixed L. Except for the results at $R = 3{\cdot}13 \times 10^4$, the trend of the data indicates that $\psi_\infty(\frac{1}{2})$ is inversely proportional to a function of R. The agreement between the observations and the numerical calculations of Stewart & Weinberg (1972) at two different values of R is good. For aspect ratios larger than unity the observations show that the core stream function $\psi_\infty(z)$ increases as R increases, see figures 14 and 15. It is apparent that

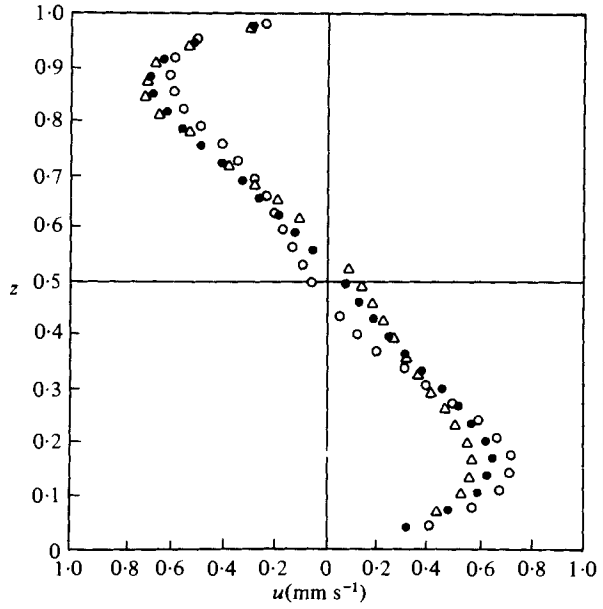

FIGURE 12. Velocity distribution as a function of location, $R = 7{\cdot}47 \times 10^5$, $L = 4$, $\Delta T = 35{\cdot}4$ °C, $\nu = 10$ cSt. x' (mm): ○, 59·6; ●, 39·3; △, 19·9.

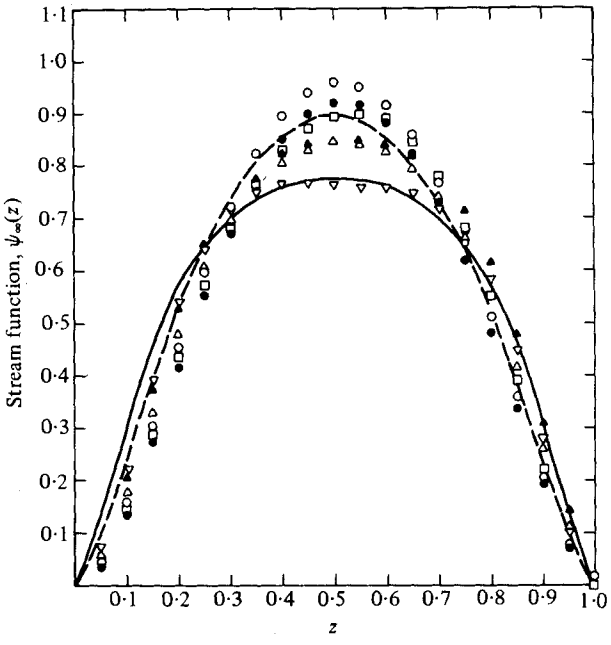

FIGURE 13. Absolute values of the core stream function for different Rayleigh numbers, $L = 1$. (R, ν, ΔT): ●, ($3{\cdot}13 \times 10^4$, 100, 4·50); ○, ($6{\cdot}16 \times 10^4$, 100, 8·85); □, ($1{\cdot}23 \times 10^5$, 100, 17·70); △, ($3{\cdot}67 \times 10^5$, 10, 4·43); ▲, ($7{\cdot}34 \times 10^5$, 10, 8·85); ▽, ($1{\cdot}47 \times 10^6$, 10, 17·75). Stewart & Weinberg, $\sigma = 10$: - - -, $R = 2 \times 10^5$; ——, $R = 2 \times 10^6$.

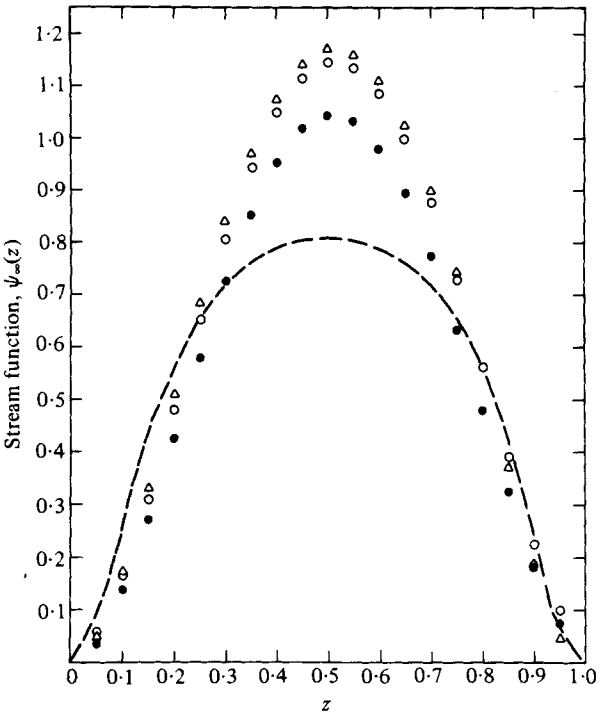

FIGURE 14. Absolute values of the core stream function for different Rayleigh numbers, $L = 2$, $\nu = 100$ cSt. $(R, \Delta T)$: ●, $(3{\cdot}1 \times 10^4, 8{\cdot}9)$; ○, $(6{\cdot}1 \times 10^4, 17{\cdot}7)$; △, $(1{\cdot}2 \times 10^5, 35{\cdot}4)$. · · ·, Quon.

these data represent some other regime than that given in figure 13 since the variation of ψ_∞ with R in the two cases is opposite. Figure 16 shows a similar increase in the core stream function when R is constant and L increases. In each of these figures the numerical results due to Quon ($L = 1$, $R = 8 \times 10^5$) are given as a reference, not for quantitative comparison.

A composite plot of $\psi_\infty(\frac{1}{2})$ versus R with L as a parameter is given in figure 17 together with a numerical prediction of de Vahl Davis (1968). The data illustrate the existence of two distinct regimes. For a given value of L it can be seen that for $R \sim O(10^6)$ the magnitude of $\psi_\infty(\frac{1}{2})$ is only weakly R-dependent. However, when $R \sim O(10^4)$ $\psi_\infty(\frac{1}{2})$ increases rapidly in proportion to R. In this latter region the effects on conduction are significant. Batchelor (1954) proposed that when the flow field is conduction-dominated ($R \to 0$) the stream function can be expanded in a power series, the leading term of which is given by

$$\psi_1' \sim R[1 + (1/L)^4]^{-1}.$$

Thus, in the present notation

$$\psi_1' R^{-\frac{1}{4}} \sim R^{\frac{3}{4}}[1 - (1/L)^4 + \ldots]$$

for $L \gg 1$. Hence when conduction is significant the tendency is for $\psi_\infty \sim \psi_1' R^{-\frac{1}{4}}$ to increase with R. This trend is different from the behaviour in the boundary-layer regime, where ψ_∞ decreases slowly as R increases.

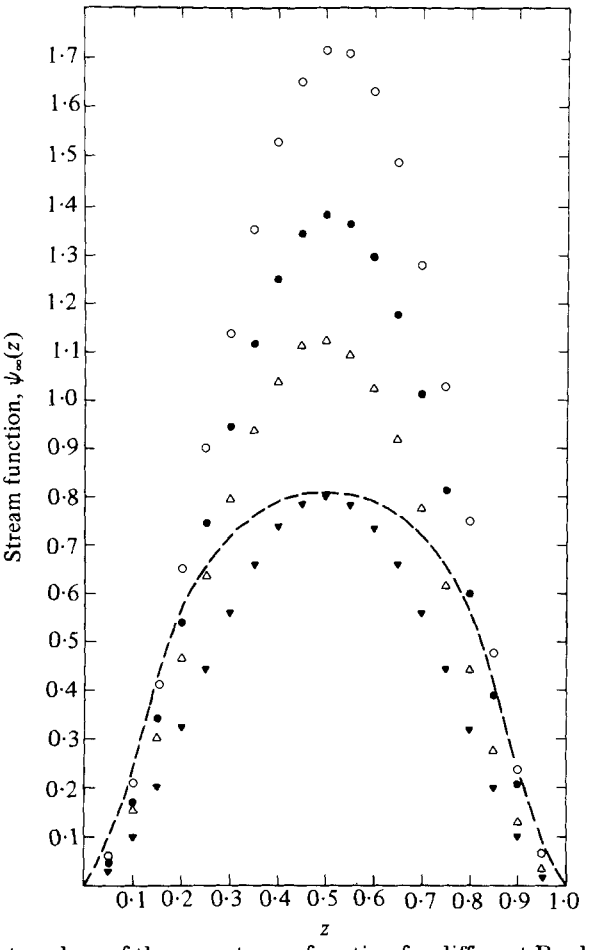

FIGURE 15. Absolute values of the core stream function for different Rayleigh numbers, $L = 8{\cdot}9$, $\nu = 100$ cSt. $(R, \Delta T)$: ▼, $(7{\cdot}1 \times 10^3, 8{\cdot}85)$; △, $(1{\cdot}6 \times 10^4, 19{\cdot}8)$; ●, $(2{\cdot}8 \times 10^4, 35{\cdot}4)$; ○, $(6{\cdot}1 \times 10^4, 76{\cdot}0)$. - - -, Quon.

Examination of the results computed by Stewart & Weinberg (1972) for $L = 1$ reveals that conduction effects are significant for values of R at least $O(10^4)$, see their figures 3 and 4. The data presented in figure 17 indicate that for the two largest aspect ratios there is little L-dependence in this region. Within the experimental scatter the two sets of data appear to be coincident, but have a gradient different from that given by de Vahl Davis (1968). The present observations correlate with the relationship $\psi_\infty(\frac{1}{2}) \sim 0{\cdot}06R^{0{\cdot}3}$, whereas the linear regime of the prediction given by de Vahl Davis behaves as $\psi_\infty(\frac{1}{2}) \sim 0{\cdot}0035R^{0{\cdot}62}$. Further, it is found that scaling $\psi_\infty(\frac{1}{2})$ by $L^{-\frac{3}{8}}$ reduces the core mass flux in the boundary-layer regime to a constant: this scaling differs from that used in § 2.

In contrast to the Batchelor model, the boundary-layer-regime models (i.e. Singh & Cowling 1963; Gill 1966; Blythe & Simpkins 1977) make a directly opposite assumption, namely that the mass flux in the vertical boundary layers is large. These models lead to a core flow field which is vertically stratified and sheared, consistent with the experimental observations in cavities for $L < 1$ (see Eckert & Carlson 1961; Elder

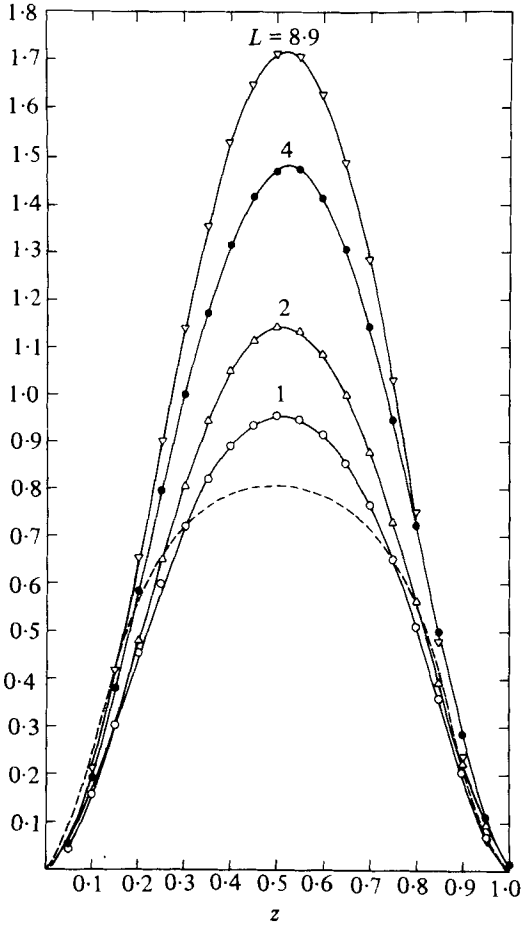

FIGURE 16. Core stream functions for various aspect ratios and $R = 6{\cdot}4 \pm 0{\cdot}4 \times 10^4$, $\nu = 100$ cSt. ○, $R = 6{\cdot}2 \times 10^4$; ●, $R = 6{\cdot}8 \times 10^4$; △, ▽, $R = 6{\cdot}1 \times 10^4$. - - -, Quon.

1965; Seki, Fukusako & Inaba 1978). The solutions for the vertical boundary layer and the core in this regime are, to first-order, independent of R and L in the limit $\sigma \gg 1$, as noted earlier. The experimental results at fixed R and σ are strongly L-dependent, for $L > 1$, which suggests that the effect of the boundary layers on the horizontal walls cannot be neglected when the motion is predominantly horizontal. Even in the boundary-layer regime, $R > O(10^5)$, where ψ is only a weak function of R, the aspect ratio dependence is most pronounced. It would appear, therefore, that, for $L > 1$, the horizontal layers impose a more stringent constraint on the limitations of the boundary-layer regime than that suggested by Gill. The observations at fixed L, which show ψ to be only a weak function of Rayleigh number and lateral position, agree with the boundary-layer models for which $\psi_\infty = \psi(z)$ in the core. Furthermore the results in figure 13, which include those given in figure 10, imply that the horizontal boundary layers get thinner as $R \to \infty$ at constant L. Consequently, the influence of the horizontal boundary layers on the core in such circumstances is reduced. However, it is conceivable that a transition to turbulence might occur before this limit is achieved

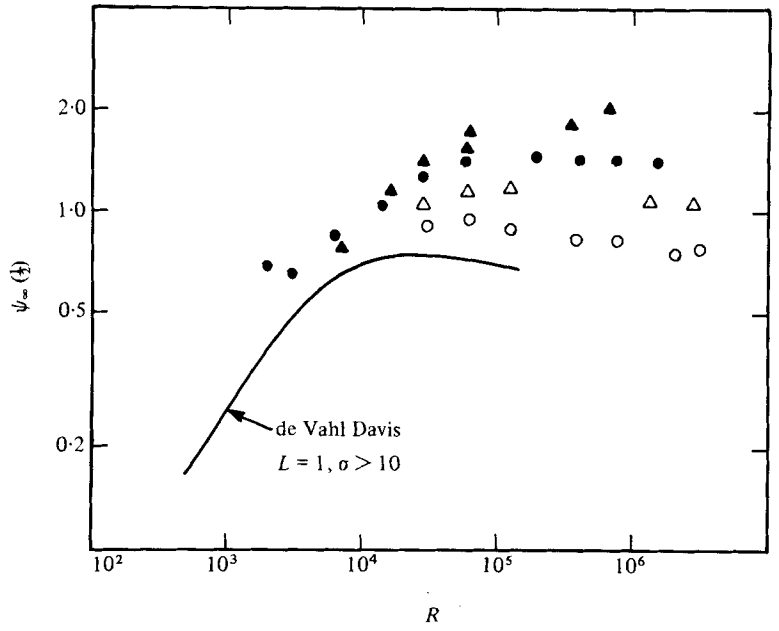

FIGURE 17. Mid-point stream function dependence on R and L. ▲, L = 8·9; ●, L = 4·0; △, L = 2·0; ○, L = 1·0.

when $L > 1$. The weak R-dependence observed in figure 17 for $R > 10^5$ represents a second-order correction to the boundary-layer models.

4.5. *The transitional flow field*

Experiments complementary to those under discussion have been reported by Elder (1965) and Seki *et al.* (1978) for the limiting case $L \ll 1$. All of that work has found that for $R \leqslant 10^3$ the basic flow structure is a single two-dimensional cell. For $R > 10^3$ some similarities occur between the present observations and the earlier work, but there are also noticeable differences. Perhaps the most substantial difference between the observations is the form of the secondary flows that develop with increasing Rayleigh number. When $L \ll 1$ the unicellular structure degenerates into a secondary flow composed of a series of vertically aligned parallel rolls that completely fill the core. As the Rayleigh number is increased further the weak shear layer between successive secondary rolls develops a tertiary flow in the form of a weak vortex. The circulation in the primary and secondary flows is in the same direction and in the opposite sense to that in the tertiary vortices.

In the present observations the secondary flow that develops takes the form of two horizontally aligned parallel rolls that, in general, do not fill the core. An exception occurs when $L = \frac{1}{2}$, where the core is observed to be initially filled by the secondary flow. At the other aspect ratios where the secondary flows were observed the core ultimately appears to develop into a turbulent state as R increases. There is no evidence of more than two secondary rolls appearing when the aspect ratio is increased. Within the limits of this study therefore the situation equivalent to the $L \ll 1$ limit, for which there might appear successive secondary rolls aligned horizontally, has not

been observed. Rather, the secondary rolls remain near the outer edges of the vertical boundary layers and the motion between them becomes disordered. As the Rayleigh number increases subsidiary vortices† appear with the secondary rolls and their effect on the core flow becomes more and more pronounced as they intensify. This behaviour is illustrated in the photographs of figure 4 when $R > 10^6$. The circulation in both the primary and secondary flows is in the same direction. After the onset of the subsidiary motion some of the circulation is in the opposite sense as the transition to turbulence develops. Seki *et al.* (1978) refer to this state as a transitional regime. They have observed the intense subsidiary vortices near the vertical walls of a cavity when $L = 0{\cdot}167$ and $R \sim O(10^{10})$.

Elder suggests that the secondary motion occurs in slender cavities at a critical Rayleigh number given by

$$R_c L^4 \sim 3 \times 10^5 \pm 30\,\%.$$

The measurements of Seki *et al.*, also for slender cavities, are in reasonable agreement with Elder's prediction. The present experimental observations do not correlate with the above expression when $L \geqslant 1$. In these cases the critical Rayleigh number at which secondary rolls near the vertical walls occur, is given by

$$R_c L^{\frac{1}{2}} \sim 6{\cdot}4 \times 10^5 \pm 10\,\%,$$

which has an aspect-ratio dependence different from the slender cavity data. It should again be emphasized, however, that the motion in the cavity at supercritical Rayleigh numbers is quite different for $L \ll 1$ and $L \geqslant 1$.

5. Conclusions

The results of this study of free convection in cavities with aspect ratios $0{\cdot}25 \leqslant L \leqslant 9$ containing fluids with Prandtl numbers $\sigma \geqslant 10$ can be summarized as follows:

(i) For $R < O(10^5)$ the conduction effects are significant and the core appears to be proportional to a function of R but independent of L.

(ii) Gill's prediction that, after appropriate co-ordinate scaling, the vertical boundary-layer solutions are independent of the Rayleigh number and the aspect ratio is confirmed.

(iii) For $R > O(10^5)$, the primary flow field remains unicellular. When $L = 1$, the numerical results are in good agreement with the observed velocity distributions.

(iv) In the boundary-layer regime, the scaled core stream function is proportional to a function of the aspect ratio and, to first order, independent of R for $L > 1$. This dependence is not implied by the leading-order boundary-layer approximation, which suggests that ψ_∞ is independent of R and L. Since the influence of the horizontal layers is neglected in the present boundary-layer models, it is suggested that the role played by these layers is significant when $L > 1$.

(v) The critical Rayleigh number at which secondary rolls occur does not agree with the Elder data for tall slender cavities. For aspect ratios $L \geqslant 1$ the critical Rayleigh number is given by

$$R_c L^{\frac{1}{2}} \sim 6{\cdot}4 \times 10^5 \pm 10\,\%.$$

† The subsidiary vortices should not be confused with the tertiary motion described by Elder and Seki *et al.* In that work the tertiary vortices occur in the shear layer *between* the successive rolls of the secondary motion.

(vi) An instability in the secondary motion develops with increasing Rayleigh number. Subsidiary vortices evolve near the vertical walls and a transition to turbulence appears in the core.

We thank Professor P. A. Blythe, Center for the Application of Mathematics, Lehigh University, for a number of helpful discussions.

Appendix A. Scalings for the boundary-layer profiles

The notation used below is consistent with that of Blythe & Simpkins (1977). The similarity boundary-layer profiles in non-dimensional co-ordinates are given as

$$w(z,\eta) = -A(z)F(\eta),$$

where $A(z) = \psi_\infty(z)/\delta(z)$ and $\eta = x/\delta(z)$. In the above expressions ψ_∞ is the core stream function, δ is a boundary-layer thickness and x is the horizontal distance from the vertical wall, all appropriately non-dimensionalized. To relate these normalized variables to the observations of the vertical velocity component w' at location and x' recall the scalings used earlier:

$$w = (h/\kappa)R^{\frac{1}{4}}w', \quad x = R^{\frac{1}{4}}(x'/h),$$

where κ is the thermal diffusivity and h the cavity height.

In the similarity solutions discussed by Blythe & Simpkins, it was found that

$$A(z) = -K^{-\frac{1}{3}}b^{\frac{1}{2}}L^{\frac{1}{2}}\psi_\infty^{\frac{2}{3}}T_\infty^{\frac{1}{3}},$$

and the boundary-layer thickness

$$\delta(z) = K^{\frac{1}{3}}b^{\frac{1}{4}}L^{-\frac{1}{4}}(\psi_\infty/T_\infty)^{\frac{1}{3}},$$

where $K = F''(0)$, $b = K^{-\frac{4}{3}}F'''(0)$ and a scaling $\psi_\infty \to L^{\frac{1}{4}}b^{\frac{3}{4}}\psi_\infty$ has been introduced. Furthermore, the functions $G(\eta)$ and $H(\eta)$ in equation (2.5) are related to $F(\eta)$ by

$$G(\eta) = 1 - \{F''(\eta)/F''(0)\}$$

and

$$H(\eta) = \int_0^\eta F(s)\,ds.$$

Note also that $F(\eta)$ is normalized such that

$$\int_0^\infty F(\eta)\,d\eta = 1.$$

Once the function $F(\eta)$ is chosen, the constants K and b are known and the core stream function and temperature can be found as shown in the earlier work. Possible boundary-layer profiles were discussed in Blythe & Simpkins and a suitable choice was found to be

$$F(\eta) = 2e^{-\eta}\sin\eta,$$

which is used in §2. For this profile $a = 0{\cdot}25$, $b = 0{\cdot}630$, $K = 4$ and $\psi_\infty(\frac{1}{2}) = 0{\cdot}941$, which therefore give the boundary-layer thickness

$$\delta(\tfrac{1}{2}) = 1{\cdot}746L^{-\frac{1}{4}}.$$

Thus the appropriate scalings are given by

$$\eta = x/\delta = 0{\cdot}573(RL)^{\frac{1}{4}}(x'/h),$$

and

$$F(\eta) = 2{\cdot}624(RL)^{-\frac{1}{2}}(hw'/\kappa).$$

Appendix B. Physical properties of the silicone oils

The fluids used in the experiments are commercially available Union Carbide L-45 silicone oils. The table below is a reduced version of Bulletin no. F-42033A (Union Carbide Corp. 1970). The specific heat information, C_p, is taken from an earlier Bulletin no. PIB45-28 (1965). The dynamic viscosity, thermal diffusivity and Prandtl number are computed from the preceding properties.

$\nu \times 10^2$ (cm^2 s^{-1})	ρ (g cm^{-3})	$\alpha \times 10^3$ (°C^{-1})	$k \times 10^4$ (cal cm^{-1} °C^{-1})	C_p (cal g^{-1} °C^{-1})	$\kappa \times 10^3$ (cm^2 s^{-1})
10	0·94	1·08	3·06	0·34	0·957
100	0·97	0·97	3·55	0·35	1·046
500	0·973	0·97	3·63	0·35	1·066
1000	0·973	0·97	3·63	0·37	1·008

Typical properties of Union Carbide Silicone fluid L-45 at 25 °C.

REFERENCES

Batchelor, G. K. 1954 *Quart. Appl. Math.* **12**, 209.

Blythe, P. A. & Simpkins, P. G. 1977 In *Physico-Chemical Hydrodynamics* (ed. D. B. Spalding), vol. 2, p. 511. Advance Pub. Inc.

Cole, G. S. & Winegard, W. C. 1964 *J. Inst. Metals* **93**, 153.

Cormack, D. E. & Leal, L. G. 1974 *Phys. Fluids* **17**, 1049.

Cormack, D. E., Leal, L. G. & Imberger, J. 1974 *J. Fluid Mech.* **65**, 209.

de Vahl Davis, G. 1968 *Int. J. Heat Mass Transfer* **11**, 1675.

Eckert, E. R. G. & Carlson, W. O. 1961 *Int. J. Heat Mass Transfer* **2**, 106.

Elder, J. W. 1965 *J. Fluid Mech.* **23**, 77.

Gill, A. E. 1966 *J. Fluid Mech.* **26**, 515.

Gill, A. E. 1974 *J. Fluid Mech.* **64**, 577.

Hadley, G. 1735 *Phil. Trans. Roy. Soc.* **29**, 58.

Hart, J. E. 1972 *J. Atmos. Sci.* **29**, 687.

Hurle, D. T. J. 1966 *Phil. Mag.* **13**, 305.

Hurle, D. T. J., Jakeman, E. & Johnson, C. P. 1974 *J. Fluid Mech.* **64**, 565.

Joseph, D. D. 1976 *Stability of Fluid Motions II*, p. 3. Springer.

Landau, L. D. & Lifshitz, E. M. 1959 *Fluid Mechanics*, cha. V, §56. Addison-Wesley.

Müller, A. & Wilhelm, M. 1964 *Z. Naturforsch.* **19a**, 254.

Pamplin, B. R. & Bolt, G. H. 1976 *J. Phys.* D, *Appl. Phys.* **9**, 145.

Quon, C. 1972 *Phys. Fluids* **15**, 12.

QUON, C. J. 1977 *Trans.* C, *J. Heat Transfer, A.S.M.E.* **99**, 340.
ROUX, B., GRONDIN, J. C., BONTOUX, P. & GILLY, B. 1978 *Numerical Heat Transfer* **1**, 331.
SEKI, N., FUKUSAKO, S. & INABA, H. J. 1978 *J. Fluid Mech.* **84**, 695.
SIMPKINS, P. G. & BLYTHE, P. A. 1980 *Int. J. Heat Mass Transfer* **23**, 881.
SINGH, K. R. & COWLING, T. G. 1963 *Quart. J. Mech. Appl. Math.* **16**, 17.
STEWART, M. J. & WEINBERG, F. 1972 *J. Crystal Growth* **12**, 217.
UTECH, H. P. & FLEMINGS, M. C. 1966 *J. Crystal Growth* **13**, 651.
WALKER, K. L. & HOMSY, G. M. 1978 *J. Fluid Mech.* **87**, 449.